Extraction characteristics of a dual fiber compound cavity

T. B. Simpson

Jaycor/Titan
3394 Carmel Mountain Road
San Diego CA, 92121

A. Gavrielides, P. Peterson

Air Force Research Laboratories,
Directed Energy Directorate
Nonlinear Optics Center of Technology, AFRL/DELO
3550 Aberdeen Ave. SE, Kirtland AFB, NM 87117-5776
peterson@bimbo.plk.af.mil
FAX: 505-846-1191

Abstract: We study experimentally the time dependence, steady state behavior and spectra of a dual fiber-laser compound cavity. Theoretically we confirm the CW and spectral characteristics. This particular cavity is formed with two Er-doped fiber amplifiers, each terminated with a fiber Bragg grating, and coupled through a 50/50 coupler to a common feedback and output coupling element. The experiment and theory show that a low Q, high gain symmetric compound cavity extracts nearly 4 times the power of a component resonator. This extraction is maintained even when there is significant difference in the optical pathlengths of the two component elements. Further, our measurements and theory show that the longitudinal modes of the coupled cavity are distinct from the modes of the component cavities and that the coherence is formed on a mode-by-mode basis using these coupled-cavity modes. The time behavior of the compound cavity shows slow fluctuations, on the order of seconds, consistent with perturbations in the laboratory environment.

OCIS codes: (140.3410) Laser resonators;(060.2320) Fiber optics amplifiers and oscillators

References and links

1. See, for example, V. V. Apollonov, S. I. Derzhavin, V. I. Kislov, V. V. Kuzminov, D. A. Mashkovsky and A. M. Prokhorov, "Phase-locking of the 2D Structures," Opt. Express **4**, 19 (1999), http://www.opticsexpress.org/abstract.cfm?URI=OPEX-4-1-19.
2. P. K. Cheo, A. Liu, and G. G. King, "A High-Brightness Laser Beam from a Phase-Locked Multicore Yb-doped Fiber Laser Array," IEEE Photon. Technol. Lett. **13**, 439 (2001).
3. E. J. Bochove, "Theory of Spectral Beam Combining of Fiber Lasers," IEEE J. Quantum Electron. **38**, 432 (2002).
4. V. A. Kozlov, J. Hernandez-Cordoero, and T. F. Morse , "All-fiber Coherent Beam Combining of Fiber Lasers," Opt. Lett. **24**, 1814 (1999).
5. A. E. Siegman, *Lasers*, (University Science Books, Mill Valley CA, 1986.)

1 Introduction

Coupling of multiple lasers into a single coherent source as a method for achieving a high-power, high-brightness source remains a persistent problem in optics. Coherent

#1456 - $15.00 US Received July 30, 2002; Revised September 23, 2002

coupling is particularly attractive for compact, rugged, high efficiency semiconductor- or fiber-based lasers which have output powers limited by the small transverse dimensions of the gain medium. Coherent combining methods include phase control, stimulated Brillouin scattering, four-wave mixing, and other nonlinear processes. Generally, these techniques require additional optical elements that are external to the gain element, such as phase correctors, scattering cells, and these these techniques usually include free space propagation. A distinct method of creating a coherent beam from multiple gain elements, and one that is easily adaptable to an all-fiber or other guided-wave laser configuration, is a compound cavity. In such a configuration, intracavity coupling is used to enforce coherence between gain elements; for example, semiconductor lasers are coherently combined using Talbot-effect cavities [1]. More recently fiber lasers are attracting considerable attention as a high-power, solid-state laser system, and there are efforts underway to combine multiple elements into a compact, spatially coherent source [2, 3].

In its basic form a compound resonator consists of gain elements which share common intra-cavity beam combining elements. To make this clear we refer to fig. (1) which shows the schematic for our mathematical development. This version of a compound cavity consists of two gain elements both supporting forward propagating fields F_i, reverse fields B_i and each with a separate small signal gain G_i, $i = 1, 2$. The reflectivity on the right end of the amplifiers is 100%. At the beam splitter (BS), these beams interfere with the forward F and reverse B propagating fields in the bare common cavity which in turn terminates with an output coupler with intensity feedback reflectivity R^2. For simplicity we restrict the common cavity to be free of gain. The beam splitter is characterized by a field reflectivity and transmission of r and t with $r^2 + t^2 = 1$. Note that the length of the two gain cavities l_i and the common cavity L are all different. This feature is particularly relevant to fiber lasers where the long gain medium makes it practically impossible to match cavity lengths on the scale of an optical wavelength. At the beam splitter the interference between these beams can range from completely constructive to completely destructive depending on the cavity lengths and the cavity longitudinal modal propagation constant k_i. Thus, the losses through the field E_{BS} differ for each cavity mode. Note that because of the shared cavity both gain elements experience the same mode spectra; hence the designation of 'compound cavity'.

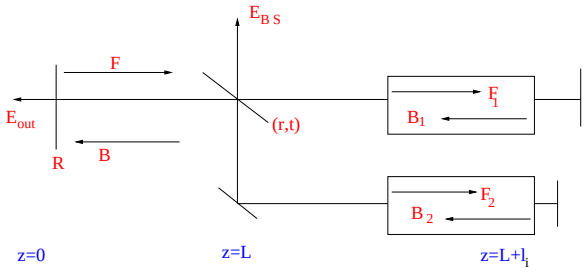

Fig. 1. Diagram and nomenclature for the compound cavity.

The utility of intracavity coupling of fiber lasers was recently demonstrated by studying their spectral combining properties [4]. This particular compound cavity [4] was formed with two single-mode Erbium (Er)-doped fiber amplifiers, each with a high reflectivity fiber Bragg grating (FBG) as a back mirror, coupled through one-half of a 2×2 fused taper single-mode coupler that acted as the compound cavity output coupler. The coupler was cleaved at the center of the interaction region. This configuration provided

#1456 - $15.00 US
Received July 30, 2002; Revised September 23, 2002

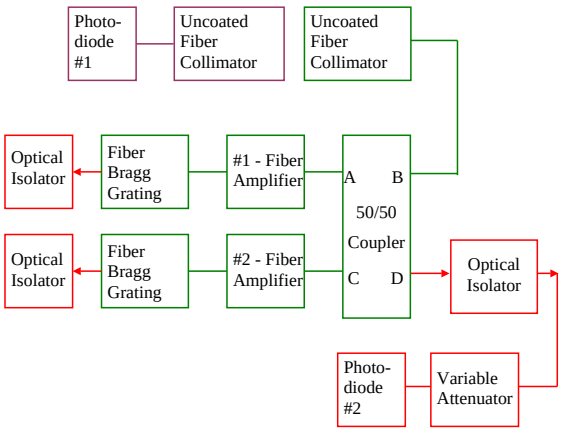

Fig. 2. Schematic of the fiber compound cavity. Additional lengths of fiber can be inserted between the FBGs and the amplifiers, and polarization control elements between the amplifiers and the 50/50 coupler.

a straightforward method to couple multiple elements through a common aperture. In this experiment multiplexing was emphasized, thus the input fiber Bragg gratings for the two lasers had slightly different resonant wavelengths. Additionally, they looked at the criteria for injection locking. However, they did not assess extraction or the modal and coherence properties of this type of compound cavity.

Here, we demonstrate that a coupled fiber-amplifier configuration can spontaneously generate a highly coherent output with longitudinal mode characteristics that differ from the modes of the component lasers. We show that when two identical fiber amplifiers are coupled through a standard 50/50 fiber coupler they spontaneously operate on modes that maximize the constructive interference of the fields within the coupler. These measurements are combined with our analytical modeling to give a consistent picture of the intracavity coupling. In the following we first describe the experimental configuration, apparatus and results. Then we develop an analytical model. Finally, we conclude by comparing the two and showing agreement.

2 Experiment

Our experiment corresponding to fig. (1) is an all-fiber arrangement shown in fig. (2). The fiber is single transverse mode, with a mode pattern compatible with industry standard SMF-28 fiber. Each gain leg is an independent Er-doped fiber terminated with a high reflector fiber Bragg grating. Cladding-pumped Er-doped fiber amplifiers provide the gain and have a length of approximately 10m. Separate pumping to each amplifier is provided by laser diodes under independent bias control. The small signal gain of the amplifiers is so high, up to 40 dB, that there is quite a bit of flexibility in the insertion of intracavity elements. Independent fiber components are connected using FC/APC connectors to minimize stray back-reflection while maintaining ease of reconfiguration. The FBGs are commercially available products specified to operate as a high reflector on one of the 100 GHz wide channels of the ITU grid. The gratings used in these experiments were fabricated for the grid channel at 1557nm. Approximately 2 meters of fiber pigtail and an FC/APC connector separate the gratings from the amplifier elements. Additional lengths of fiber can be inserted at the connector point. The mutual

#1456 - $15.00 US
Received July 30, 2002; Revised September 23, 2002

coupling is through the 50/50 fiber coupler; this corresponds to the beam splitter in fig. (1). Approximately 2 meters of fiber separates the coupler from the amplifier elements. The common cavity originates at port B and terminates on an uncoated fiber collimator that provides about 4% back reflection into the cavity and acts as the common output coupler. The length of the fiber in the common cavity is about 2m. The field exiting port D, termed E_{BS}, is lost from the cavity. Optical isolators prevent stray back reflections into the cavity.

Photodiode #1 monitors the output transmitted through the fiber collimator after being collected at a second fiber collimator and is a measure of E_{out} of figure (1). This photodiode has a bandwidth of greater than 10GHz allowing broadband power spectra to be generated using a microwave spectrum analyzer. Optical spectra also are generated using a heterodyne technique with a distributed feedback laser diode acting as the local oscillator. By ramping the bias current of the laser diode the optical frequency of the local oscillator is swept over a range of approximately 25 GHz with a spectral resolution of approximately 100 MHz. This detector also provides a signal proportional to the average output power, with a bandwidth of a few kHz. This lower bandwidth signal is compared with the output of a second photodiode, photodiode #2 in figure (2), that monitors the optical power lost from the cavity at port D to measure E_{BS}. The temporal characteristics of these signals were monitored using a digitizing oscilloscope.

We did not use polarization-maintaining fiber in the compound cavity but did manipulate the polarization. Initally, we simply twisted a fiber and clamped it down. Later we used commercial polarization control components inserted between the fiber amplifiers and the fiber coupler (not shown in fig. 2). Polarization alignment at the coupling element was important for achieving a high degree of coherence between the output of the two gain legs of the coupled cavity. However, a single adjustment is sufficient for data taken over several hours. Using commercially available components in the configuration shown in fig. (2), the two component laser cavities had path lengths that could be matched within 1 cm. We also introduced length differences of up to approximately 33% by inserting lengths of passive fiber. The cavity mode spacing without additional fiber is approximately 6MHz corresponding to optical path length of about $16m \times 1.53 = 25$m in each leg. Because the mode spacing for the isolated lasers is approximately 6 MHz, this resolution does not permit the isolation of individual modes in the optical spectrum. However, we observed that the lasers operated on more than one mode simultaneously. Therefore, we investigated the individual mode characteristics by monitoring the power spectrum of the photodetected signal. Optical and power spectra of the solitary component lasers showed an output consists of only a sparse set of modes with significant optical power. Typically only $10-20$ dominant modes appear out of the approximately 10^4 available modes within the high-reflection band of the fiber Bragg grating. Similar optical spectra occur under coherent coupling, except that isolated modes become mode clusters of multiple peaks within the 100 MHz resolution of the optical spectra.

Figure (3) shows the photodetector output from the uncoated fiber collimator for both of the two component lasers, and the compound configuration. A component laser is a result of turning off the pump laser diode to one of the fiber amplifiers. The Er-doped fiber of the unpumped amplifier is then a strong absorber so that, depending upon the component laser under test, port A or C of the fiber coupler becomes a second loss port. Coherence is evident in the compound cavity since its output is approximately four times that of one of the isolated amplifiers. We consider the origin of this factor of four in more detail following eq. (14). Thus, almost all of the optical power exits the feedback surface and very little is lost through port D of the 50/50 beam coupler. A second feature of the output characteristics is that the time variation is relatively slow, corresponding to laboratory thermal changes, for example. Temporal changes corresponding to the time

#1456 - $15.00 US Received July 30, 2002; Revised September 23, 2002

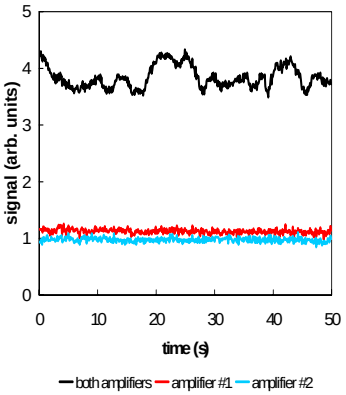

Fig. 3. Time dependence of the compound (black) and component cavities (colored).

scale of the relaxation resonance (sub-millisecond) or the cavity mode spacing (sub-microsecond) were relatively small. However, there were significant power fluctuations on nanosecond and sub-nanosecond time scales, corresponding to the mode beating of the dominant modes.

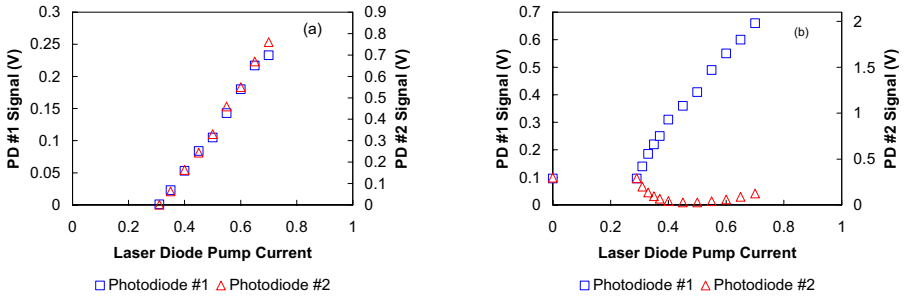

Fig. 4. (a) The extraction curves for the component cavities. (b) outcoupled power, left axis, and the power exiting the beam splitter, right axis for the compound cavity. The pump current is in amps.

Next we consider the steady state characteristics of the compound cavity. As a reference we begin with the component fiber amplifier. Fig. (4a) shows the outputs of a single component cavity as monitored by both photodiodes as a function of the pump current. The threshold is near 0.3 amp and the extraction is linear; that is, there are no higher order processes like excited state absorption. In Fig (4b) amplifier #2 is pumped until the signal from photodiode #1 reaches .1 Volt. Subsequently this component laser remains fixed and the ordinate in fig(4b) shows the pumping to amplifier #1. As this pumping increases the output remains constant until threshold is reached at the component laser threshold of .3Amps. After this point the signal from the collimator grows while the photodiode signal from the loss port D goes through a minimum. The minimum occurs when the amplifiers are pumped to a similar output level. Note that the

#1456 - $15.00 US
Received July 30, 2002; Revised September 23, 2002

signal measured by photodiode number #1 is approximately four times, not two times, the single laser signal; see the discussion after eq. (14). In this case almost all of the power is coupled to the fiber collimator and less than 10% is coupled through loss port D. Because the fused fiber coupler diverts the optical power based on the field characteristics in the interaction region, the direction of the optical power to one output arm requires a high degree of coherence between the two input beams. If we manipulate the polarization, we can achieve the situation where essentially equal output power to ports B and D is achieved in the coupled cavity configuration. This is expected for orthogonal polarizations of the input to the fiber coupler.

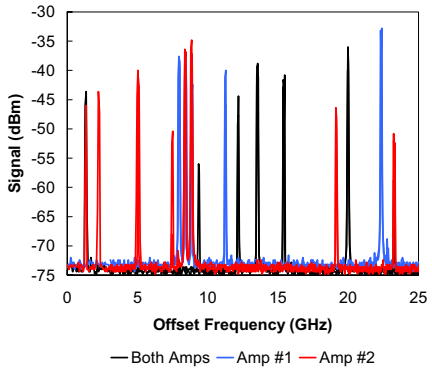

Fig. 5. Spectra of the component (colored) and the compound cavity (black).

Typical optical spectra for the two component amplifiers (colored) and the coupled configuration (black) are shown in fig. (5). Because the high reflection bandwidth of the FBGs is approximately 100GHz only part of the optical spectra is shown. The laser oscillates on several modes simultaneously but these modes come and go continuously on a time scale on the order of seconds. This time scale is consistent with small environmental changes in the laboratory, and the time scale of power fluctuations of the coupled cavity.

Finally, mode beating spectra that give information about individual modes are shown in Figures 6 and 7. Figure 6 shows one mode beating frequency for the case when the two component cavities are nearly equal. It shows the mode-beating spectrum of the 79th harmonic of the fundamental mode frequency. To generate this spectra, the microwave spectrum analyzer is set on its "peak hold" setting that saves the highest power level at each frequency and the curves are generated over time as the laser modes randomly changed. Note that the frequencies of the peaks for the two component lasers are offset and that the peak of the compound cavity lies between them. The offset between the two component-laser frequencies corresponds to a fractional cavity-length mismatch of approximately 0.0008, or approximately 1 cm. With larger cavity mismatches a high degree of coherence is still maintained in the compound cavity. Figure 7 shows the mode beating spectra for the case when an additional 5 meters of fiber, corresponding to approximately a 0.3 fractional change in length, is added to one of the component cavities. Again, the "peak hold" setting of the spectrum analyzer is used to generate the spectra. Now the individual mode spectra differ and the compound-cavity modes are quite distinct from the component cavity modes. However, high output power is observed only on those compound cavity modes that are also simultaneously near resonant with

#1456 - $15.00 US
Received July 30, 2002; Revised September 23, 2002

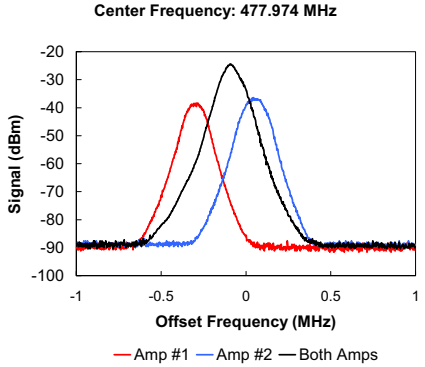

Fig. 6. Frequency offset of the 79^{th} harmonic for both component lasers and the compound laser.

a cavity mode from each of the two component cavities.

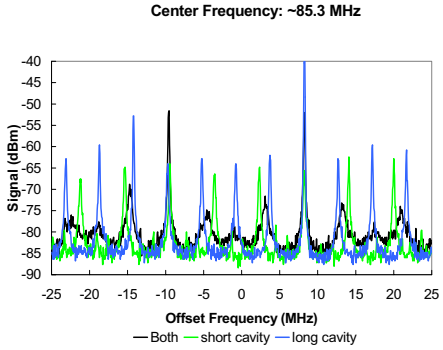

Fig. 7. Mode beating spectra of the two component cavities and the compound cavity. One of the two components cavities has approximately 5 meters of additional fiber inserted. The spectrum analyzer is operating on its "peak hold" setting and the spectra shown here are accumulated over a period of a couple of minutes with the beating frequencies filling in as the laser randomly changed oscillation modes. Note that the compound cavity only showed strong output on those modes that are simultaneously nearly resonant with the two component cavity modes.

In summary, the two-laser compound cavity is robust, and over 90% of the output is coherently coupled from the cavity through the common output coupler. The mutual locking of the two lasers occurs on a mode-by-mode basis and the cavity mode frequencies of the coupled cavity differ from those of the component cavities. In passing, we mention that we also built a four-element version of figure (2) using a tree-type configuration of fiber couplers. Preliminary results with this configuration showed a much higher sensitivity to fluctuations in the laboratory environment, and typically only around 75% of the power was outcoupled and the power fluctuations were large.

#1456 - $15.00 US
Received July 30, 2002; Revised September 23, 2002

3 Theory

In this section, with the details relegated to the appendix, we derive the steady state resonator eigenvalue equation, the outcoupled power, and the power exiting the beam splitter as functions of the gains G_i, beam splitter reflectivity r^2, output reflectivity R^2, and the three different cavity lengths l_i, L. We begin with the complex gain equation in the Rigrod approximation [5] which we write as

$$\frac{dE_i}{dz} = \pm(\frac{g_i}{1+f_i^2+b_i^2} + ik_i)E_i \tag{1}$$

where g_i is the single pass small signal gain. E_i is either the forward going fields F_i for the plus sign, or the reverse fields B_i for the negative sign. These in turn decompose as

$$F_i(z) = f_i(z)\exp(i\phi_i(z)), \quad B_i(z) = b_i(z)\exp(i\beta_i(z)). \tag{2}$$

The boundary condtions at the beam splitter are

$$F_1(L) = itF(L), \text{ and } \mathrm{F_2(L) = rF(L)}, \tag{3}$$

$$B(L) = -itB_1(L) + rB_2(L), \; E_{BS}(L) = rB_1(L) - itB_2(L). \tag{4}$$

Also, since the common cavity is bare the forward and reverse cavity fields are related by

$$F(L) = F(0)\exp(ikL), \quad B(0) = B(L)\exp(ikL), \tag{5}$$

which is supplemented with the outcoupling boundary condition, $F(0) = RB(0)$.

The eignevalue equation which satifies eqs. (1 -5) is derived in the appendix and is

$$\begin{aligned} &r^2\left(\sin^2[\Psi(1+\delta l)] - R^2t^4\sin^2(2\Psi\delta l)\right)\left(G_2 + \ln\left[-Rr^2\frac{\sin(2\Psi\delta l)}{\sin[\Psi(1-\delta l)]}\right]\right) \\ &-t^2\left(\sin^2[\Psi(1-\delta l)] - R^2r^4\sin^2(2\Psi\delta l)\right)\left(G_1 + \ln\left[-Rt^2\frac{\sin(2\Psi\delta l)}{\sin[\Psi(1+\delta l)]}\right]\right) = 0. \end{aligned} \tag{6}$$

where the trignometric arguments are

$$\Psi = k(l_1+l_2+2L), \quad \delta l = \frac{l_2-l_1}{l_1+l_2+2L}, \text{ and } \delta = \mathrm{2k(l_2 - l_1)}. \tag{7}$$

Again, refering to the appendix eq. (A11), the amplitudes are given by

$$b_i^2 = \frac{G_i + \ln(\beta_i)}{1-\beta_i^2}, \text{ and } f_i = \beta_i b_i, \tag{8}$$

where

$$\beta_1 = Rt^2\frac{\sin(2\Psi\delta l)}{\sin[\Psi(1+\delta l)]} > 0, \text{ and } \beta_2 = -\mathrm{Rr^2}\frac{\sin(2\Psi\delta \mathrm{l})}{\sin[\Psi(1-\delta \mathrm{l})]} > 0. \tag{9}$$

A numerical solution of eq.(6) gives the periodic roots $\Psi_i, i = 0, \pm1, \pm2, ...$ The amplitude of the spectra is found by inserting these roots back into eqs.(8). It is clear that the solutions exhibit a periodicity in Ψ, and the intensities show a modulation given by $\pi/\delta l$. In the case of no coupling eq. (8) shows that the losses are determined by the logarithm of the outcoupling term R. However, for the compound cavity the losses depend on Ψ, the propagation constant of each longitudinal mode. Therefore, threshold for a specific longitudinal mode depends critically on the value of the propagation constant.

#1456 - $15.00 US
Received July 30, 2002; Revised September 23, 2002

Next, we derive the output powers. The power extracted from the output coupler is

$$\begin{aligned} I_{out} =&(1-R^2) < |B(0)|^2 >= (1-R^2) < |B(L)|^2 > \\ =&(1-R^2) < |-itB_1(L) + rB_2(L)|^2 > . \end{aligned} \tag{10}$$

Likewise the intensity exciting the cavity via the common beam splitter is

$$I_{BS} =< |rB_1(L) - itB_2(L)|^2 > . \tag{11}$$

In eqs.(10,11) all the fields are expanded in terms of longitudinal modes identified by the solution to the eigenvalue equation, eq. (6). It is assumed that the detectors are slow and the frequency components corresponding to beating between longitudinal modes are not resolved. Thus, upon averaging the above equations only the terms of the same frequency are retained. Consequently, the diagonal terms give

$$I_{out} = (1-R^2)\sum_m [t^2(b_1^m)^2 + r^2(b_2^m)^2 + 2rtb_1^m b_2^m \cos(2\Psi\delta l)], \tag{12}$$

and

$$I_{BS} = \sum_m [r^2(b_1^m)^2 + t^2(b_2^m)^2 - 2rtb_1^m b_2^m \cos(2\Psi\delta l)]. \tag{13}$$

If a single amplifier is disconnected, see fig.(2), the output intensity per mode of the remaining component fiber is

$$I_{component} = (1-R^2)t^2 \frac{G_i + \ln(t^2 R)}{1-t^4R^2}, \quad i = 1 \text{ or } 2, \tag{14}$$

as can be seen from eqs. (8,9,12).

These equations are the foundation for the power extraction analysis. The maximum extractable incoherent intensity from both isolated resonators is $I_{incoh} = \Sigma I_i$ where $I_i = G_i + \ln(R)$, $i = 1, 2$. The conditions for maximum coherent output power clearly requires that the resonator must be symmetric with $t^2 = r^2 = 1/2$ and $G_1 = G_2 = G$. Further, eq. (12) and the following equations show that as both δl and R^2 become small the ratio I_{out}/I_{incoh} is less than but approaches unity for arbitrary gain. That is, under these two conditions the total available incoherent power from the two isolated lasers is extracted as a coherent beam. However, if δl or R^2 is not small, say near 10% then this ratio is less than unity. Similarly, under the two above conditions of smallness the ratio of $I_{out}/I_{component}$ is greater than 4 and only approaches 4 as the gain becomes large. These are our experimental conditions as shown in fig. (3). Again, if δl or R^2 is greater than about 10% or the gain is small this ration deviates from 4; a large gain would be greater than about 15. Thus, in order to extract the maximum coherent power the compound resonator must have a low Q and be symmetric.

Before leaving the theoretical development we consider two special cases of the eigenvalue equation. The first case is for the single cavity specified by either $r = 0$ or $t = 0$ in eq. (6). Picking the former condition gives $\Psi(1-\delta l) = n\pi$, for $n = 0, \pm1, \pm2, ...$ However, eq.(9) requires that $\beta_1 = (-1)^n R > 0$. Therefore, only even values of n contribute to non trivial longitudinal modes in agreement with expectations. Thus, eq. (7) leads to

$$\Delta\nu_n = \frac{c}{2\pi}(k_{n+1} - k_n) = \frac{c}{2(l_1 + L)}, \text{ with } b_i^2 = \frac{G_i + \ln R}{1-R^2} \tag{15}$$

which is in agreement with the usual single resonator conditions. Similar results hold if $t = 0$. The second case is identical amplifiers characterized by $G_1 = G_2$, $r = t = 1/\sqrt{2}$, however $l_1 \neq l_2$. From eq. (6) we find that

$$\sin[\Psi(1+\delta l)] = -\sin[\Psi(1-\delta l)]. \tag{16}$$

#1456 - $15.00 US Received July 30, 2002; Revised September 23, 2002

This equation has two solutions. The first is $2\Psi\delta l = \pi + 2n\pi$ which leads to the nonlasing solution $\beta_1 = \beta_2 = 0$. The second solution is $\Psi = n\pi$, $n = 0, \pm 1, \pm 2, ...$ which leads to $\beta_1 = \beta_2 = R(-1)^n \cos(n\pi\delta l)$. Thus, since β_i must be positive, $\cos(n\pi\delta l)$ is positive for even n, and $\cos(n\pi\delta l)$ is negative for n odd. Therefore, the mode are separated by exactly 2π except at the transition from negative to positive where the separation of the modes is 3π. We note that our simulations show this behavior. In this case the mode separation is

$$\Delta\nu_n = \frac{c}{2\pi}(k_{n+1} - k_n) = \frac{c}{(l_1 + l_2 + 2L)} \approx \frac{c}{2(l_1 + L)}, \text{ for } \mathrm{l_1} \approx \mathrm{l_2} \tag{17}$$

except at the transition from n even to n odd. Thus, for the case of a nearly identical gain regions, $l_1 \approx l_2$ in eq. (7), the mode spacing is, again, determined by the component round trip length. Finally, we note that the modes are situated at $\nu_m = mc/(2(l_1 + l_2 + 2L))$, $m = 1, 2, 3....$ However, the complexities of the spectra I^m_{out} are largely determined by the interference term $(1 + \cos(2\Psi\delta l))$ in eq. (12). In both cases the allowable modes are restriced by $\beta_1 = \beta_2 = R(-1)^n \cos(n\pi\delta l) > 0$.

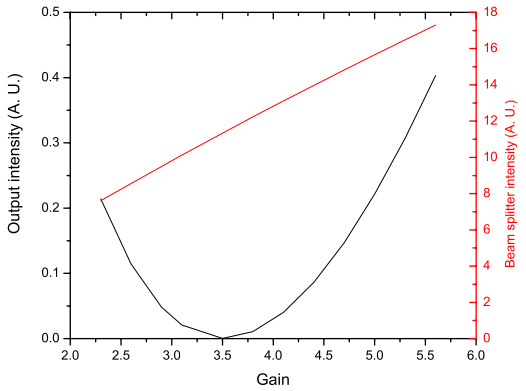

Fig. 8. Simulated extraction curves for the compound cavity. The red line is the outcoupled power and the black curve is power exiting the beam splitter.

4 Comparison

In this section we first examine our experiment by simulating fig. (4b) and by illustrating the spectra near and above threshold. Then, we investigate the more general changes in extraction as different parameters are altered. Prior to presenting these results we list the experimental parameters. The cavities lengths are $l_1 = 14$m, $l_2 = l_1 + .01m$, $L = 2$m; the index-of-refraction is 1.53. This gives $\delta l = .03\%$. The reflectivities are $R^2 = 4\%$, $r^2 = t^2 = 50\%$. The gains G_1 and G_2 are in the neighborhood of 8 for a small signal gain of about 40dB. Threshold gain $G_{th} = 2.3$ as can be seen from eq. (14) for $I_{component} = 0$. Our first result comes from eq. (17) which gives a mode spacing of 6MHz which agrees with our experiment.

Fig. (8) shows the steady state outcoupled power, I_{out}, and the exiting beam splitter power I_{BS} as a function of the gain. This figure is obtained by solving the eigenvalue equation, eq(6) for Ψ_n and then inserting these values into the spectrum equation, eq. (8), and the exiting intensity equations eqs. (12,13). To conform with the experimental

#1456 - $15.00 US
Received July 30, 2002; Revised September 23, 2002

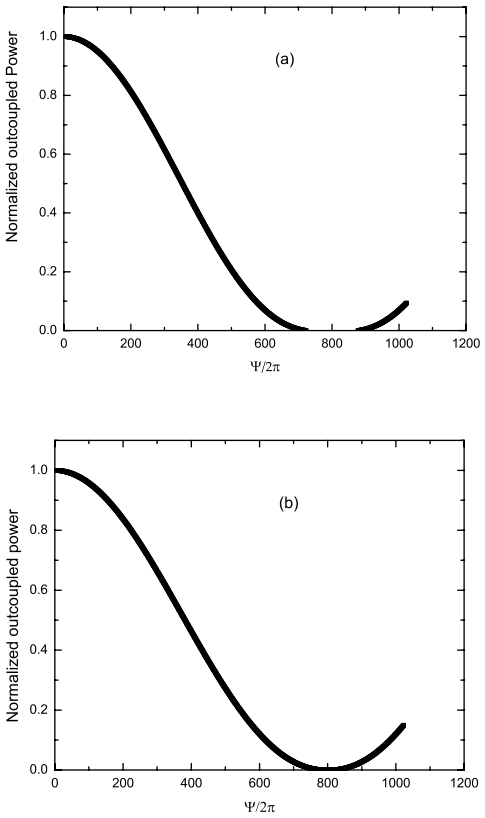

Fig. 9. (a) Output spectra just above threshold. (b) Output spectra far above above threshold. The power is normalized to the total incoherent power.

data, see fig. (4b), we set $G_1 = 3.5$ which is about 1.5 times above threshold. Then G_2 is varied from just above threshold, $G_2 = 2.5$, to a value of $G_2 = 5.3$. This interval corresponds to the experiment. Note, in our simulations we allow 3 modes to run which is again consistent with the experiment. Both figs. (4b,8) clearly show a minimum in the beam splitter power when the two gains are equal; that is the resonator is symmetric as the theory predicts. Further, for a gain of 3.5 $I_{component}$, see eq.(14), has a value of 1.8. Thus, from fig. (8) the ratio $I_{out}/I_{component}$ is 6.4 which is greater than the value of 4 shown in fig. (3). The difference is attributable to more losses in the experiment than have been accounted for in the model.

Next we consider the spectra in more detail. Figs. (9a,9b) shows the outcoupled power, the summand in eq. (12), as a function of $\Psi_n/2\pi$. Figure (9a) is near threshold for $G_1 = G_2 = 3.5$ and fig. (9b) is well above threshold for $G_1 = G_2 = 8$. Both graphs are normalized to the available incoherent power $I_{incoh} = \Sigma I_i$ where $I_i = G_i + \ln(R)$, $i = 1, 2$. Both graphs clearly show the modulation $\Psi_{mod} = \pi/2\delta l = 1,600$ which gives a frequency of $\nu_{mod} = c/2n\Delta l = 10$Ghz for $\Delta l = .01$m. The distinguishing feature is that modes near $\nu_{mod}/2$ experience destructive interference and do not lase for small gains, but appear at larger gains. Although this figure does not resolve the mode spacing a closer look show that $\Delta\Psi_n/2\pi$ is an integer and gives a $\Delta\nu = c/(l_1 + l_2 + 2L) = 6$Mhz spacing.

#1456 - $15.00 US
Received July 30, 2002; Revised September 23, 2002

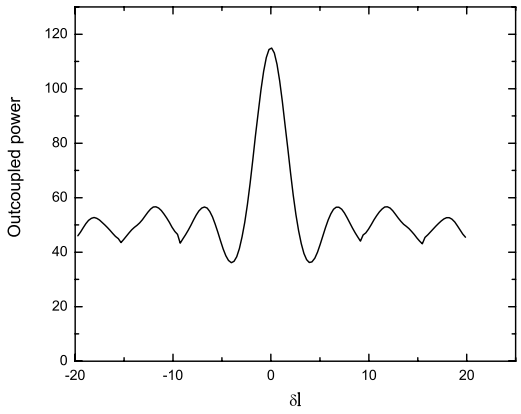

Fig. 10. Power output as a function of δl

Our last subject is the outcoupled power as a function of detuning $\delta l = (l_1 - l_2)/(l_1 + l_2 + 2L)$. Fig. (10) shows the output power I_{out} given by eq. (12) as a function of $\delta l\%$ for $r^2 = .5$, $G_1 = G_2 = 8$ and $r^2 = .04$; note that we are still allowing only 3 modes as before. The graph is symmetric about the maximum output of 115 which occurs at $\delta l = 0$. The maximum output drops by 15% for a relative length difference of $\delta l = .03\%$. If the outcoupling is increased to $R^2 = .5$ the maximum is increased to a value of 138, but the remainder of the graph stays as in fig. (10). Also, we mention that our simulations show that for a change in r^2 of 20% results in a decrease of the $\delta l = 0$ peak of about 2%. Thus, the reflectivity as well as the path lengths do not have to be accurately specified.

5 Summary

We have constructed a dual element fiber compound cavity using a 50/50 coupler. One port of the coupler is a loss port; another is connected to the common cavity and the two remaining adjacent ports are connected to the Erbium fibers which are terminated with fiber Bragg gratings. We showed that the outcoupled power is about 4 times that of a single fiber laser when the only significant difference between the two fibers is their lengths. We also showed that the mode spacing of the compound laser is determined by the single pass optical lengths of the two component cavities. The insertion of the beam splitter causes the compound mode frequency to be distinct from the mode frequencies of the two component lasers.

Appendix

In this section we outline the derivation for the eigenvalue and spectral equations. There are three consequences of the complex gain equation, see eqs. (1,2). The first result is the differential equation for the amplitudes

$$\frac{df_i}{dz} = \frac{g_i}{1 + f_i^2 + b_i^2} f_i. \tag{A1}$$

The second consequence is the constant relation between the forward and reverse amplitudes: $f_i(z)b_i(z) = \text{constant} = \mathrm{f_i(L)b_i(L)} = \mathrm{f_i(L + l_i)b_i(L + l_i)}$. The third prop-

#1456 - $15.00 US
Received July 30, 2002; Revised September 23, 2002

erty comes from the imaginary part of eq. (1) and gives $\phi_i(L) - \phi_i(L + l_i) = k_i l_i$ and $\beta_i(L + l_i) - \beta_i(L) = k_i l_i$. However, at $z = L + l_i$ the phase is preserved, that is $\phi(L+l_i) = \beta(L+l_i)$ since the imposed field boundary condition is $F_i(L+l_i) = B_i(L+l_i)$. Thus,

$$\beta_i(L) - \phi_i(L) = 2k_i l_i, \tag{A2}$$

as expected.

The amplitude growth equation is found by integrating and applying the boundary conditions, $F_i(L + l_i) = B_i(L + l_i)$, to eq. (A1). This gives

$$\ln \frac{b_i^2(L)}{f_i^2(L)} + [b_i^2(L) - f_i^2(L)] = 2g_i L_i \equiv G_i. \tag{A3}$$

We now look at the boundary conditions in more detail. Eqs. (3.4,5) when combined gives the connection between the forward and reverse fields in each leg as

$$F_1(L) = itR(-itB_1(L) + rB_2(L)) \exp(2ikL), \tag{A4}$$

$$F_2(L) = rR(-itB_1(L) + rB_2(L)) \exp(2ikL). \tag{A5}$$

Further more the amplitudes and phases at the beam splitter are constrained by dividing eqs. (3), thus

$$\frac{f_1}{f_2} = \frac{t}{r}, \quad \text{and} \quad \exp(i(\phi_1(L) - \phi_2(L)) = i. \tag{A6}$$

The relations between the reverse fields and the forward fields are derived by combining eqs.(A4,A5,A6). From the imaginary part, the reverse fields satisify

$$b_1 = Cb_2, \quad \text{where} \quad \mathrm{C} = -\frac{\mathrm{r}\,\sin[\Psi(1 + \delta\mathrm{l})]}{\mathrm{t}\,\sin[\Psi(1 - \delta\mathrm{l})]} > 0 \tag{A7}$$

with the trigonometric arguments

$$\Psi = k(l_1 + l_2 + 2L), \quad \delta l = \frac{l_2 - l_1}{l_1 + l_2 + 2L}, \quad \text{and} \quad \delta = 2\mathrm{k}(\mathrm{l}_2 - \mathrm{l}_1). \tag{A8}$$

Ψ is the single trip optical path difference (OPD) which determines the frequency of the mode, δl is the normalized gain length mismatch, and δ is the OPD mismatch.

The real part of eqs.(A4,A5) gives the equations between the forward and reverse gain amplitudes as

$$f_1 = \beta_1 b_1, \quad \text{where} \quad \beta_1 = \mathrm{Rt}^2 \frac{\sin(2\Psi\delta\mathrm{l})}{\sin[\Psi(1 + \delta\mathrm{l})]} > 0, \tag{A9}$$

and

$$f_2 = \beta_2 b_2, \quad \text{where} \quad \beta_2 = -\mathrm{Rr}^2 \frac{\sin(2\Psi\delta\mathrm{l})}{\sin[\Psi(1 - \delta\mathrm{l})]} > 0. \tag{A10}$$

Next inclusion of the growth equation, eq. (A3), supplemented by eqs. (A6-A8) yields the classic equation relating the gain/loss terms given by

$$b_i^2 = \frac{G_i + \ln(\beta_i)}{1 - \beta_i^2}. \tag{A11}$$

Finally by eliminating the amplitudes in the above equations gives the eigenvalue equation

$$\begin{aligned} &r^2 \left(\sin^2[\Psi(1 + \delta l)] - R^2 t^4 \sin^2(2\Psi\delta l)\right) \left(G_2 + \ln\left[-Rr^2 \frac{\sin(2\Psi\delta l)}{\sin[\Psi(1 - \delta l)]}\right]\right) \\ &-t^2 \left(\sin^2[\Psi(1 - \delta l)] - R^2 r^4 \sin^2(2\Psi\delta l)\right) \left(G_1 + \ln\left[-Rt^2 \frac{\sin(2\Psi\delta l)}{\sin[\Psi(1 + \delta l)]}\right]\right) = 0. \end{aligned} \tag{A12}$$

#1456 - $15.00 US Received July 30, 2002; Revised September 23, 2002

This equation is solved for the variables Ψ_i and consequently k_i through eq.(A8). Note, however, that all physical solutions Ψ_i must also satisfy the above three inequalities eqs.(A7,A9,A10)

#1456 - $15.00 US Received July 30, 2002; Revised September 23, 2002